P1.1 ANNOUNCING THE SHEBA BULK TURBULENT FLUX ALGORITHM

Edgar L Andreas[1*], P. Ola G. Persson[2,3], Andrey A. Grachev[2,3], Rachel E. Jordan[4], Peter S. Guest[5], Christopher W. Fairall[2], Thomas W. Horst[6], and Jian-Wen Bao[2]

[1]NorthWest Research Associates, Lebanon, New Hampshire
[2]NOAA Earth System Research Laboratory, Boulder, Colorado
[3]Cooperative Institute for Research in Environmental Sciences, University of Colorado, Boulder, Colorado
[4]U.S. Army Cold Regions Research and Engineering Laboratory, Hanover, New Hampshire
[5]Naval Postgraduate School, Monterey, California
[6]National Center for Atmospheric Research, Boulder, Colorado

1. INTRODUCTION

We call ourselves the SHEBA Atmospheric Surface Flux Group (ASFG). SHEBA was the year-long experiment in the Beaufort Gyre to study the Surface Heat Budget of the Arctic Ocean (Uttal et al. 2002). A main goal of our participation in SHEBA was to develop a bulk turbulent flux algorithm—comparable in style and simplicity to the COARE algorithm (Fairall et al. 1996, 2003)—to accurately predict the turbulent surface fluxes of momentum and sensible and latent heat over sea ice (Andreas et al. 1999). We are pleased to announce the release of version 1.0 of that bulk flux algorithm.

Our SHEBA observations ran for almost a year—from late October 1997 through the end of September 1998. For analysis purposes, we divided the SHEBA year into just two aerodynamic seasons: winter and summer (Andreas et al. 2003; cf. Brunke et al. 2006). Figure 1 shows our motivation for this division. We explain more about our data and our analysis later. For now, you just need to know that Fig. 1 shows nominal 10-day averages of hourly values of the 10-m, neutral-stability drag coefficient, C_{DN10}, for six of our SHEBA sites.

A key feature of Fig. 1 is that from mid-May through mid-September the five sites depicted all behave quite consistently: C_{DN10} starts relatively low, increases to a maximum as the amount of open water increased during summer, then decreases as the open water froze and the ice surface collected snow. We attribute this behavior in C_{DN10} during summer to form drag caused by the vertical flow edges associated with the melt ponds and leads. "Summer" in our SHEBA data set ran from 15 May through 14 September 1998.

The remainder of the SHEBA year—from the start of our measurements in late October 1997 through 14 May 1998 and from 15 September through the last of our measurements in late September 1998—we term "winter." In winter, the ice was compact and snow-covered, and the snow was dry enough to drift and blow in response to the wind. In summer, the snow at SHEBA was too wet to move under wind forcing and eventually disappeared altogether.

Our bulk flux algorithm treats the SHEBA winter and summer data with different parameterizations for momentum transfer. The summer parameterization is also appropriate for any marginal ice zone. The other components of our bulk flux algorithm are the same in winter and summer.

2. BULK FLUX ALGORITHM

Energy budget studies or atmospheric models with sea ice as the lower boundary almost always estimate the surface fluxes of momentum (τ) and sensible (H_s) and latent (H_L) heat from a bulk flux algorithm (e.g., Maykut 1978; Jordan et al. 1999; Briegleb et al. 2004). In our algorithm, the relevant flux equations take the form

$$\tau = -\rho\overline{uw} \equiv \rho u_*^2 = \rho C_{Dr} S_r^2, \qquad (2.1a)$$

$$H_s = \rho c_p \overline{w\theta} = \rho c_p C_{Hr} S_r (\Theta_s - \Theta_r), \qquad (2.1b)$$

$$H_L = \rho L_v \overline{wq} = \rho L_v C_{Er} S_r (Q_s - Q_r). \qquad (2.1c)$$

In these, u, w, θ, and q are turbulent fluctuations in longitudinal wind speed, vertical wind speed,

[*]*Corresponding author address:* Dr. Edgar L Andreas, NorthWest Research Associates, Inc. (Seattle Division), 25 Eagle Ridge, Lebanon, New Hampshire 03766-1900; e-mail: eandreas@nwra.com.

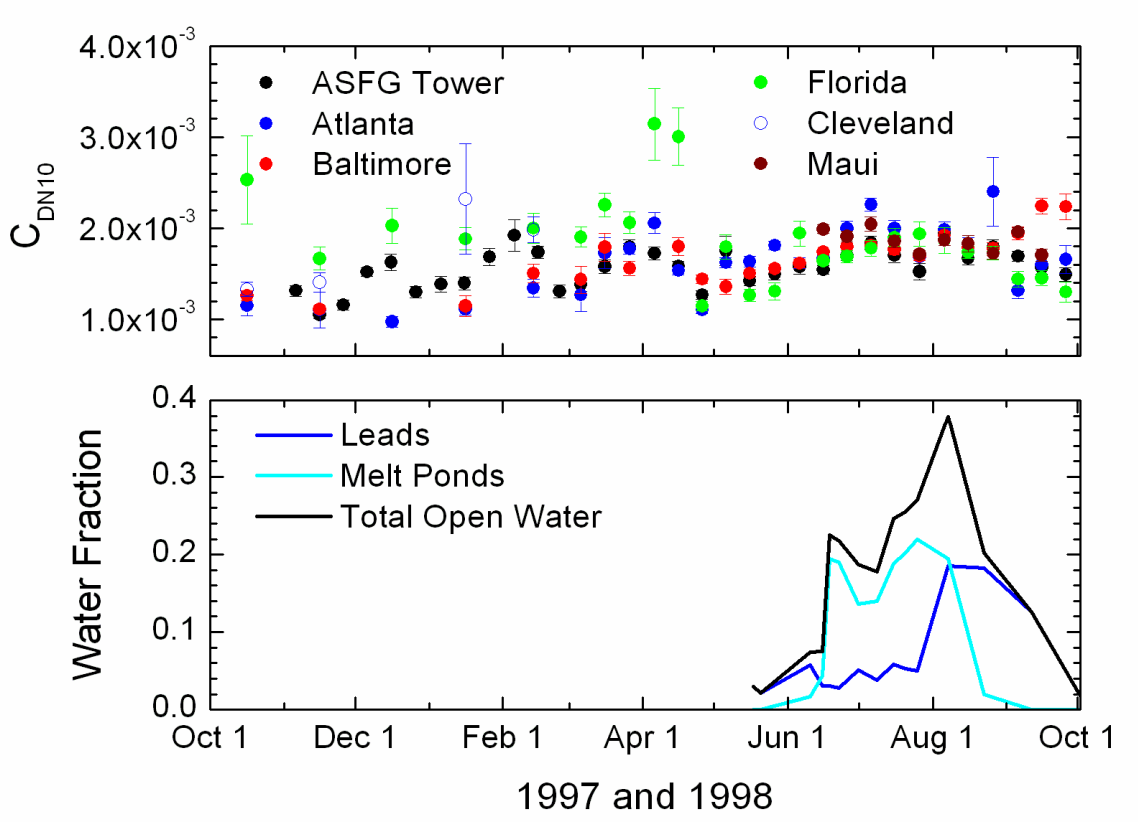

FIG. 1. The upper panel is the 10-m, neutral-stability drag coefficient obtained from hourly eddy-covariance measurements at six SHEBA sites: our main Atmospheric Surface Flux Group (ASFG) tower and five portable automated mesonet (PAM) sites named Atlanta, Baltimore, Cleveland, Florida, and Maui. Symbols represent averages of all good hourly data collected during the first 10 days of the month, the second 10 days of the month, and the final 8, 10, or 11 days of the month. Error bars represent two standard deviations in the mean. This plot summarizes over 18,500 hours of data. The lower panel shows the fractional surface area of open water in leads, in melt ponds, and the sum of the two during summer.

temperature, and specific humidity; the overbar indicates a time average. Also, ρ is the air density; c_p, the specific heat of air at constant pressure; L_v, the latent heat of sublimation; S_r, the effective wind speed at reference height r; Θ_r and Q_r, the potential temperature and specific humidity at r; and Θ_s and Q_s, the temperature and specific humidity at the surface. We evaluate Q_s as the saturation value at Θ_s. Equation (2.1a) also defines the friction velocity, u_*.

The crux of any bulk flux algorithm is evaluating the transfer coefficients for momentum, sensible heat, and latent heat appropriate for height r—respectively, C_{Dr}, C_{Hr}, and C_{Er} in (2.1). These generally derive from Monin-Obukhov similarity theory and formally are (e.g., Garratt 1992, p. 52ff.; Andreas 1998)

$$C_{Dr} = \frac{k^2}{\left[\ln(r/z_0) - \psi_m(r/L)\right]^2}, \qquad (2.2a)$$

$$C_{Hr} = \frac{k C_{Dr}^{1/2}}{\left[\ln(r/z_T) - \psi_h(r/L)\right]}, \qquad (2.2b)$$

$$C_{Er} = \frac{k C_{Dr}^{1/2}}{\left[\ln(r/z_Q) - \psi_h(r/L)\right]}. \qquad (2.2c)$$

In these, k (= 0.40) is the von Kármán constant, and ψ_m and ψ_h are empirical functions of the Obukhov length,

$$L = -\frac{\overline{\Theta}_v}{kg}\left(\frac{u_*^3}{\overline{w\theta_v}}\right). \qquad (2.3)$$

Here, g is the acceleration of gravity; $\overline{\Theta}_v$ is the surface-layer average of virtual temperature; and $\overline{w\theta_v}$ is the flux of virtual temperature.

For the stratification corrections ψ_m and ψ_h in (2.2), we use the functions from Paulson (1970) in unstable stratification and the functions from Grachev et al. (2007) in stable stratification. These latter functions are based on our SHEBA data set and include proper treatment of a heretofore unrecognized scaling regime in very stable stratification.

The z_0, z_T, and z_Q in (2.2) are the roughness lengths, respectively, for wind speed, temperature, and humidity. Developing a new parameterization for z_0 and testing Andreas's (1987) theoretical model for z_T and z_Q are the main subjects of this paper.

Finally, S_r in (2.1) is an effective wind speed. For compatibility with the COARE algorithm (Fairall et al. 1996, 2003) and other recent flux algorithms (e.g., Andreas et al. 2008), we acknowledge that in unstable stratification gustiness enhances turbulent exchange and therefore model

$$S_r = \left(U_r^2 + \beta_g^2 w_*^2\right)^{1/2}. \qquad (2.4)$$

Here, U_r is the actual measured or modeled mean wind speed at reference height r, $\beta_g = 1.25$ (Fairall et al. 1996), and w_* is Deardorff's (1970) convective velocity scale (Godfrey and Beljaars 1991):

$$w_* = u_*\left(-\frac{z_i}{kL}\right)^{1/3}, \qquad (2.5)$$

where z_i is the depth of the convective boundary layer. We take z_i as a constant, 600 m, because variability in it does not have much effect on our calculations.

We adopt the suggestion by Jordan et al. (1999) that a similar "windless" coefficient is necessary for stable stratification but express it as

$$S_r = U_r + 0.5\,\mathrm{sech}(U_r). \qquad (2.6)$$

Here, both U_r and S_r are in m s^{-1}.

Because (2.1) and (2.2) are coupled through the Obukhov length (2.3), they must be solved iteratively using the mean measured or modeled conditions: namely, U_r, Θ_r, Q_r and Θ_s. That iteration usually converges in 3 to 5 steps.

Although we focus here on the roughness lengths, these are related to the so-called neutral-stability transfer coefficients which, for a standard reference height of 10 m, are obtained from (2.2) and written as

$$C_{DN10} = \frac{k^2}{\left[\ln(10/z_0)\right]^2}, \qquad (2.7a)$$

$$C_{HN10} = \frac{k^2}{\left[\ln(10/z_0)\right]\left[\ln(10/z_T)\right]}, \qquad (2.7b)$$

$$C_{EN10} = \frac{k^2}{\left[\ln(10/z_0)\right]\left[\ln(10/z_Q)\right]}. \qquad (2.7c)$$

The C_{DN10} values calculated from (2.7a) (once we find z_0, as described later) are what we plotted in Fig. 1.

3. THE SHEBA DATA

During our SHEBA deployment, we had one central site in the SHEBA ice camp and, usually, four remote sites that ranged in distance from 0.4 to 10 km from the main camp. We serviced these remote sites about once a week. Andreas et al. (1999, 2002, 2006), Persson et al. (2002), and Grachev et al. (2005, 2007) describe the instruments that our Atmospheric Surface Flux Group deployed during SHEBA and review our data processing. Persson et al., in particular, show pictures of the instruments at our main instrument site.

The centerpiece of our site in the main SHEBA camp was a 20-m tower instrumented at five levels with identical sonic anemometer/thermometers (K-type sonics from Applied Technologies, Inc.) and Vaisala HMP235 temperature and humidity sensors. The tower also held one Ophir hygrometer that was mounted at 8 m, near the sonic at that level.

Through eddy-covariance measurements using standard turbulence processing, as described in Persson et al. (2002), Grachev et al. (2005, 2007), and Andreas et al. (2006), we measured the momentum flux τ and the sensible heat flux H_s for each of the five tower levels and the latent heat flux H_L at one level [see (2.1)]. This

latter was the only direct, long-term measurement of latent heat flux from SHEBA.

The sonics also yielded the mean wind speed U_r at each level for use in (2.4) and (2.6). The Vaisala HMP235s provided the mean temperature and specific humidity, Θ_r and Q_r, needed in (2.1).

Near this ASFG tower was a full suite of radiometers for measuring incoming and outgoing longwave and shortwave radiation and several additional sensors for measuring surface temperature, Θ_s (e.g., Claffey et al. 1999). Generally, for Θ_s we used the value implied by the emitted ($Q_{L\uparrow}$) and incoming ($Q_{L\downarrow}$) longwave radiation measured by our Eppley pyrgeometers:

$$\Theta_s = (\sigma\varepsilon)^{-1/4}\left[Q_{L\uparrow} - (1-\varepsilon)Q_{L\downarrow}\right]^{1/4} . \quad (3.1)$$

Here, ε (= 0.99) is the surface emissivity, and σ ($=5.67051\times10^{-8}\,\mathrm{W\,m^{-2}\,K^{-4}}$) is the Stefan-Boltzmann constant. See the SHEBA data archive at http://www.eol.ucar.edu/projects/sheba for tabulations and descriptions of these surface temperature data and the other data sets that we use in this study.

Our remote sites were instrumented with Flux-PAM (portable automated mesonet) stations from the National Center for Atmospheric Research instrument pool (Militzer et al. 1995; Horst et al. 1997). Our first four sites, which we deployed in October 1997, were named Atlanta, Baltimore, Cleveland, and Florida after the four teams that were playing in the Major League Baseball League Championship Series at the time. The Cleveland station was damaged by a pressure ridge in early February 1998, removed from service, and redeployed at a new site called Seattle in mid-April 1998. Seattle, however, became an untenable site because of ice motions; and this PAM station was again redeployed to a site named Maui in mid-June 1998. That Maui site lasted until late September 1998, as did the original Atlanta, Baltimore, and Florida sites.

We have found the data from Seattle to be disturbed by a pressure ridge just upwind of the station and, thus, do not include data from that site in our analysis. We do use data for the other five PAM sites, however.

Each Flux-PAM station measured at one height the same quantities that we measured at the ASFG tower: that is, wind speed and direction, temperature, relative humidity, and the turbulent fluxes of momentum and sensible heat. The website http://www.eol.ucar.edu/rtf/projects/SHEBA contains instrument details, a history of each of the PAM sites deployed during SHEBA, and information on data processing.

Briefly, the PAM stations provided hourly averaged data, as did the main tower site. Each PAM station used a sonic anemometer/thermometer mounted at a height between 2.5 and 3.5 m, depending on instrument type, to measure the turbulent fluxes of momentum and sensible heat by eddy-covariance techniques [i.e., τ and H_s in (2.1)]. We used sonics from both Gill (Solent R2) and Applied Technologies, Inc. (K-type), for the turbulence measurements at these sites.

To measure mean temperature and relative humidity at the Flux-PAM sites, we used Vaisala HMD50Y sensors in mechanically aspirated radiation shields (Andreas et al. 2002). Each PAM station also measured barometric pressure with a Vaisala PTB 220B digital barometer. Because our main ASFG site had no measurement of barometric pressure, we used the pressure data from the Florida PAM site at the tower site also because only about 400 m separated the two sites.

Each PAM station included sets of up-looking and down-looking radiometers to measure shortwave (Kipp and Zonen model CM21) and longwave (Eppley model PIR) radiation. We obtained surface temperature at the PAM sites exclusively from these longwave radiometers through (3.1).

From the turbulent fluxes and mean meteorological quantities measured at multiple levels on our main tower and at the Flux-PAM sites, we could compute the turbulent transfer coefficients C_{Dr}, C_{Hr}, and C_{Er} from (2.1). These, in turn, give us estimates of the roughness lengths from (2.2):

$$z_0 = r\exp\left\{-\left[k C_{Dr}^{-1/2} + \psi_m(r/L)\right]\right\}, \quad (3.2a)$$

$$z_T = r\exp\left\{-\left[k C_{Dr}^{1/2} C_{Hr}^{-1} + \psi_h(r/L)\right]\right\}, \quad (3.5b)$$

$$z_Q = r\exp\left\{-\left[k C_{Dr}^{1/2} C_{Er}^{-1} + \psi_h(r/L)\right]\right\}. \quad (3.5c)$$

Here, the roughness lengths are in meters if r is in meters. Moreover, solving these involves no iteration because our data also provided L. On inserting z_0 in (2.7a), we also computed the C_{DN10} values shown in Fig. 1 and in a later plot.

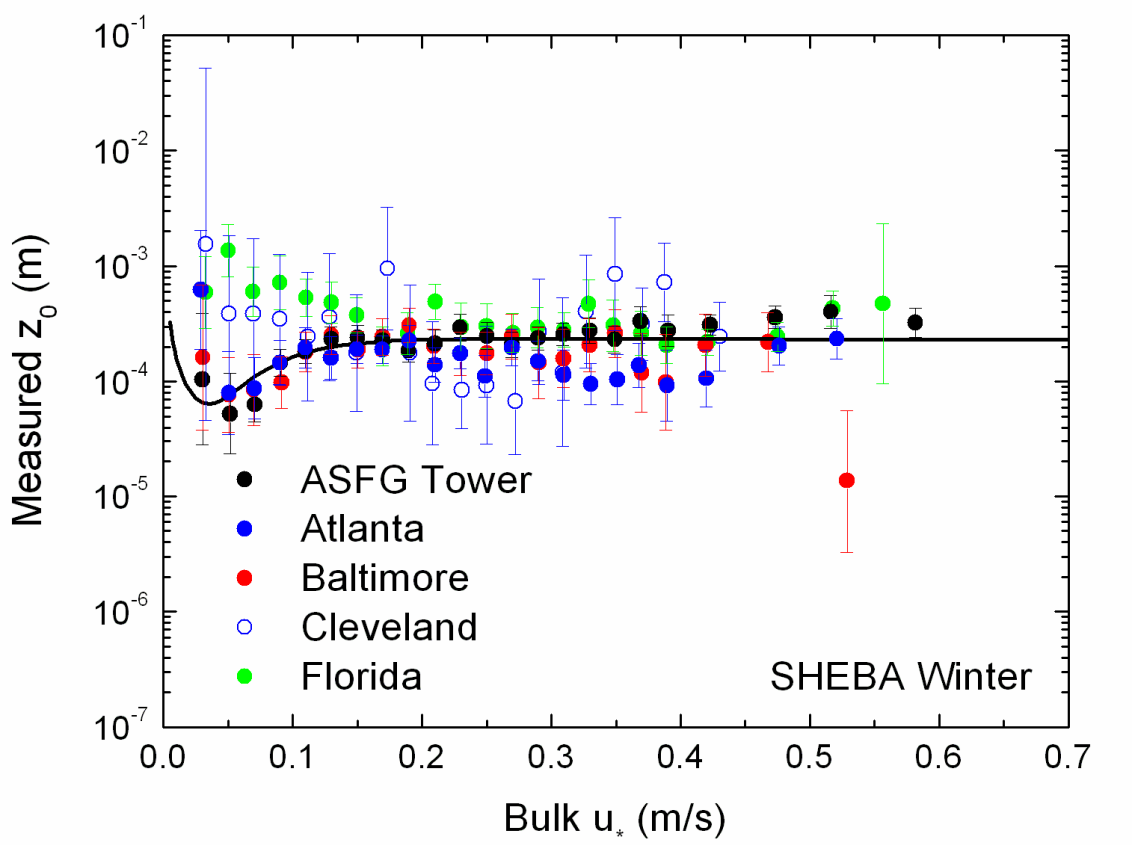

Fig. 2. Bin-averaged z_0 data from the ASFG tower and from four Flux-PAM sites are plotted against an estimate of u_* from our bulk flux algorithm, $u_{*,B}$. The $u_{*,B}$ bins are typically $2\,\mathrm{cm\,s^{-1}}$ wide; error bars are ±2 standard deviations in the bin means. The curve is (4.1). This plot summarizes over 9000 hours of data.

4. ALGORITHM FOR WINTER

In preliminary analyses of the roughness length z_0 in winter (Andreas et al. 2003, 2004), we had plotted measured z_0 against measured u_*. If u_* is measured to be erroneously large, propagating this error through (3.2a) convinced us that z_0 would be evaluated to be erroneously large. Likewise, if u_* is measured to be erroneously small, z_0 will be evaluated to be erroneously small. As a result, plots of z_0 versus measured u_* tend to have a positive slope because of shared errors. We call this fictitious correlation because it does not result from real physics. This fictitious correlation probably explains why Andreas et al. (2003, 2004) and Brunke et al. (2006) found z_0 to generally increase with u_* in earlier analyses of the SHEBA data set.

Figure 2 shows a more meaningful result. Here we plot measured z_0 against an estimate of u_* from our bulk flux algorithm. Such a representation eliminates shared errors, and we therefore anticipate minimal effects from fictitious correlation. Moreover, the objective of a bulk flux algorithm is to estimate an accurate roughness length from a bulk estimate of u_*, denoted $u_{*,B}$. That relationship is what Fig. 2 shows.

The symbols in Fig. 2 are geometric means of hourly z_0 values in $u_{*,B}$ bins that are typically $2\,\mathrm{cm\,s^{-1}}$ wide. The error bars are ±2 standard deviations in these bin means.

The curve in Fig. 2 is

$$z_0 = 0.135\frac{\nu}{u_{*,B}} + 2.30\times10^{-4}\tanh^3\left(13u_{*,B}\right), \quad (4.1)$$

where ν is the kinematic viscosity of air. Here, z_0 is in meters when the other variables have MKS units.

Equation (4.1) suggests that z_0 follows aerodynamically smooth scaling for small $u_{*,B}$.

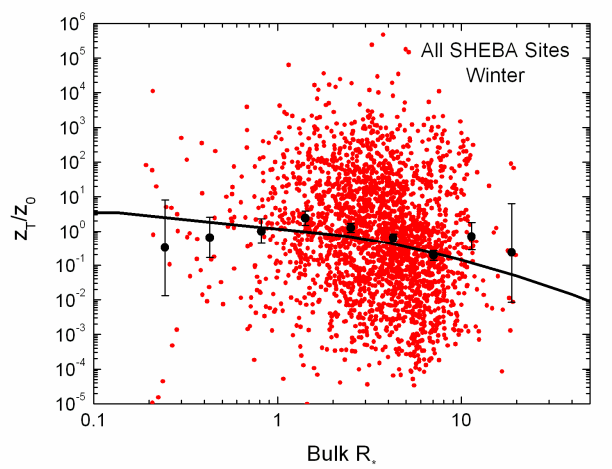

Fig. 3. Hourly measurements (2418 values) of z_T/z_0 (red circles) during winter made on the ASFG tower and at the Flux-PAM sites Atlanta, Baltimore, Cleveland, and Florida are plotted against the roughness Reynolds number from our bulk flux algorithm. The black circles are bin averages, and the error bars represent ±2 standard deviations in the bin means. The curve is Andreas's (1987) model, (4.2).

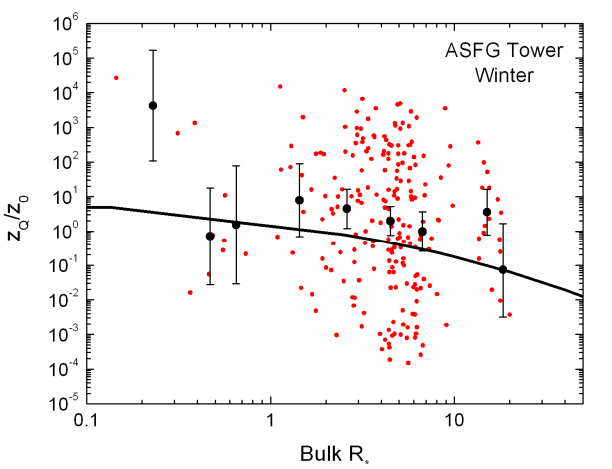

Fig. 4. As in Fig. 3, except this shows z_Q/z_0 from only one site, the Atmospheric Surface Flux Group tower. This plot summarizes 227 hours of data.

Figure 2 shows that three of the five SHEBA sites confirm this scaling. Data from the ASFG tower, Atlanta, and Baltimore show z_0 decreasing with increasing $u_{*,B}$ for $u_{*,B}$ between 0 and $0.04\,m\,s^{-1}$. The scanty data from Cleveland and the Florida data do not, however, show the minimum in z_0 associated with aerodynamically smooth flow.

As $u_{*,B}$ increases beyond $0.04\,m\,s^{-1}$, z_0 increases; but that increase is effectively over when $u_{*,B}$ reaches approximately $0.15\,m\,s^{-1}$. Beyond this limit, z_0 is essentially constant at $2.3\times10^{-4}\,m$. Our preliminary analysis had shown no aerodynamically smooth region and that z_0 increased continuously when we plotted it against the measured value of u_*.

Our candidate expression for the roughness lengths for temperature (z_T) and humidity (z_Q) is Andreas's (1987) theoretical model. This expresses the ratio z_s/z_0, where z_s is either scalar roughness (z_T or z_Q), as a function of the roughness Reynolds number, $R_* = u_* z_0 / \nu$:

$$\ln(z_s/z_0) = b_0 + b_1 \ln R_* + b_2 (\ln R_*)^2 . \quad (4.2)$$

Andreas (1987, 2002) tabulates the polynomial coefficients b_0, b_1, and b_2.

Andreas (2002) demonstrated that plots of z_T/z_0 and z_Q/z_0 versus R_*, necessary to test (4.2), where all quantities are measured, suffer from fictitious correlation such that the plotted data tend to follow the slope that (4.2) predicts. If we use a bulk flux algorithm to compute R_*, however, the measured u_* and z_0 do not appear in both dependent and independent variables, and the fictitious correlation is mitigated. Furthermore, as with z_0, we want our bulk flux algorithm to predict accurate values of z_T/z_0 and z_Q/z_0 from a bulk estimate of R_*, denoted $R_{*,B} = u_{*,B} z_{0,B} / \nu$, where $u_{*,B}$ and $z_{0,B}$ come from our bulk flux algorithm. All of our subsequent figures of scalar roughness therefore show measured z_T/z_0 or z_Q/z_0 plotted against $R_{*,B}$.

Figure 3 is the first such plot; it shows all hourly z_T/z_0 values measured at our SHEBA sites during winter and plotted against $R_{*,B}$. Andreas et al. (2009) explain the screening that we did to obtain the measured values. They also describe our study of whether z_T/z_0 and z_Q/z_0 depend on stratification. Because we found no compelling evidence that stratification affects scalar roughness, Fig. 3 and subsequent plots of scalar roughness combine data collected in both stable

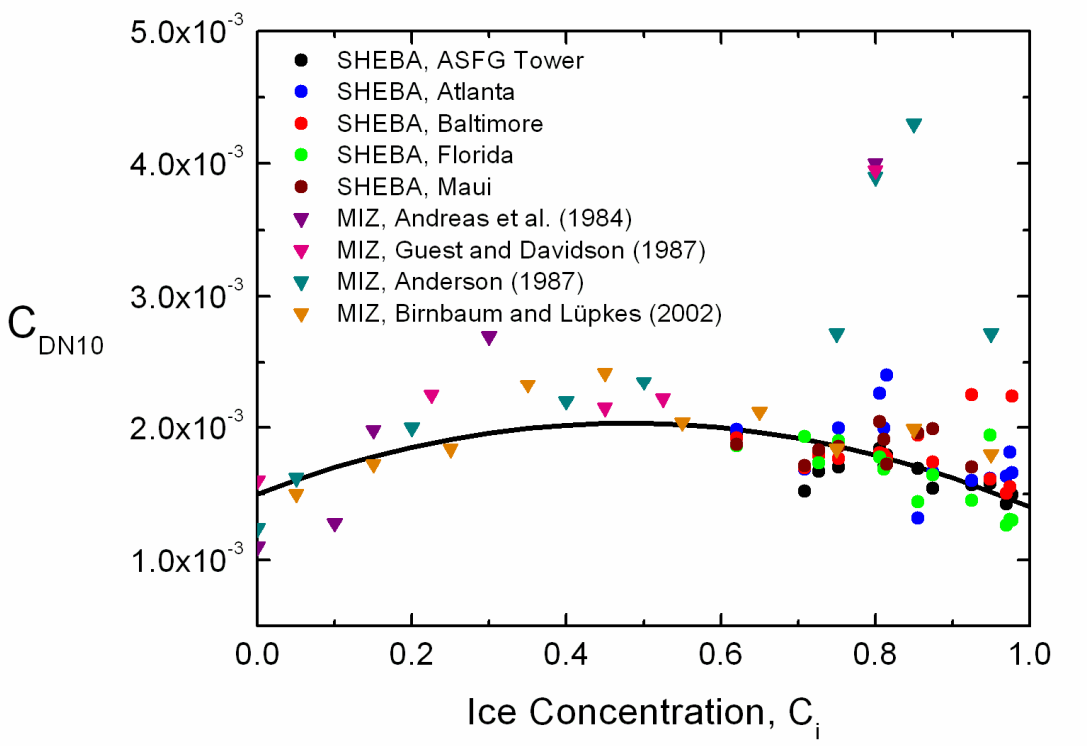

Fig. 5. The 10-day averages of summer C_{DN10} values from Fig. 1 from the ASFG tower and from the Flux-PAM sites called Atlanta, Baltimore, Florida, and Maui are plotted against ice concentration, C_i. The figure also shows C_{DN10} values obtained in the Antarctic marginal ice zone (MIZ; Andreas et al. 1984) and the Arctic MIZ (Guest and Davidson 1987; Anderson 1987; Birnbaum and Lüpkes 2002). The curve is (5.3).

and unstable stratification.

The black circles with error bars in Fig. 3 are geometric means of the hourly data in $R_{*,B}$ bins; the error bars show ±2 standard deviations in the bin means. These bin means lie very close to Andreas's (1987) theoretical model, (4.2), and, therefore, provide good confirmation for it.

Figure 4 shows a comparable plot of z_Q/z_0. Because we made only one long-term measurement of the latent heat flux during SHEBA—at the 8-m level on the ASFG tower—this figure has far fewer data than in Fig. 3. Still, the bin-averaged data agree with Andreas's (1987) model; we thus retain it as our parameterization for z_s/z_0 in winter.

5. ALGORITHM FOR SUMMER SEA ICE AND THE MARGINAL ICE ZONE

Figure 1 suggests to us that form drag associated with the vertical edges created by leads and melt ponds dominates the momentum exchange in summer. Andreas et al. (1984) had inferred that the same process is at work in the marginal ice zone (MIZ) and had therefore parameterized their observations of the drag coefficient in the MIZ as a function of ice concentration, C_i.

We have therefore associated each averaged summer drag coefficient in Fig. 1 with the ice concentration at the middle of the averaging interval and show these results in Fig. 5. If, in Fig. 1, C_P is the areal fraction of melt ponds and C_L is the areal fraction of leads, the total open water fraction plotted is

$$C_w = C_P + C_L . \qquad (5.1)$$

Consequently, in Fig. 5,

$$C_i = 1 - C_w . \qquad (5.2)$$

Figure 5 confirms our interpretation of Fig. 1: As the open water fraction increases (i.e., as C_i

decreases from 1.0), C_{DN10} values from the SHEBA set increase.

To continue this theme that momentum exchange over polar surface that are mixes of ice and open water is strongly influenced by form drag, we have added to Fig. 5 C_{DN10} values from four sets of measurements in marginal ice zones. These data span the entire range of ice concentration, 0.0 to 1.0. At low ice concentration, all four MIZ sets agree well. At high ice concentrations, Birnbaum and Lüpkes's (2002) marginal ice zone data are indistinguishable from our SHEBA data. Thus, the mere presence of both ice and water seems to produce surfaces that are aerodynamically similar.

Hence, we fitted all the C_{DN10} data in Fig. 5 with a single quadratic function of ice concentration:

$$10^3 C_{DN10} = 1.500 + 2.233 C_i - 2.333 C_i^2 . \quad (5.3)$$

This equation is thus our parameterization for the drag coefficient for summer sea ice. By inserting C_{DN10} values obtained from (5.3) into (2.7a) and inverting to obtain z_0, you can calculate the appropriate C_{Dr} from (2.2a) to use in (2.1a) to compute surface stress. Furthermore, because (5.3) recognizes the similarity between momentum exchange over summer sea ice and the marginal ice zone, it can be used for any season in the MIZ.

Over a surface that consists of three different elements, as summer sea ice does—namely, ice, leads, and melt ponds—we might presume that a mosaic approach (Andreas and Makshtas 1985; Vihma 1995) is best for estimating average heat fluxes. That is, the measured sensible heat flux (H_s), for example, would be a linear combination of the contributions from sea ice ($H_{s,i}$), leads ($H_{s,L}$) and melt ponds ($H_{s,P}$):

$$H_s = C_i H_{s,i} + C_L H_{s,L} + C_P H_{s,P} . \quad (5.4)$$

From (2.1b), we would expand this further as

$$\begin{aligned} H_s = {} & \rho_i c_{p,i} C_i C_{Hr,i} S_{r,i} \left(\Theta_{s,i} - \Theta_{r,i}\right) \\ & + \rho_L c_{p,L} C_L C_{Hr,L} S_{r,L} \left(\Theta_{s,L} - \Theta_{r,L}\right) , \\ & + \rho_P c_{p,P} C_P C_{Hr,P} S_{r,P} \left(\Theta_{s,P} - \Theta_{r,P}\right) \end{aligned} \quad (5.5)$$

where subscripts i, L, and P denote individual values appropriate over ice, leads, and melt ponds. Expressions like (5.4) and (5.5) should also apply to the latent heat flux.

Since the leads and melt ponds were fairly small, we can assume that the air at reference height r is well mixed. Thus, $S_{r,i} = S_{r,L} = S_{r,P} = S_r$ and $\Theta_{r,i} = \Theta_{r,L} = \Theta_{r,P} = \Theta_r$. Likewise, since the temperatures of the air and the various surfaces were all within a few degrees of 0°C, we can further approximate $\rho_i = \rho_L = \rho_P = \rho$ and $c_{p,i} = c_{p,L} = c_{p,P} = c_p$. These two conditions further suggest that $C_{Hr,i}$, $C_{Hr,L}$, and $C_{Hr,P}$ are all approximately equal: call the common values C_{Hr}.

With these approximations, (5.5) reduces to

$$H_s = \rho c_p C_{Hr} S_r \left(\Theta_{s,Ave} - \Theta_r\right) , \quad (5.6)$$

where

$$\Theta_{s,Ave} = C_i \Theta_{s,i} + C_L \Theta_{s,L} + C_P \Theta_{s,P} . \quad (5.7)$$

Andreas et al. (2005) attempted to evaluate z_T from the ASFG tower data on the basis of (5.6) and (5.7). They found, however, that $\Theta_{s,Ave}$ differed, in general, so little from $\Theta_{s,i}$ that using (5.7) did not appreciably reduce the scatter in z_T/z_0 values obtained simply by using $\Theta_{s,i}$ in (5.6). In other words, we found that, over summer sea ice, a mosaic approach was of no benefit because of the similarity in all air and surface temperatures. We therefore based our subsequent values of z_T and z_Q on just the measured ice surface temperature, $\Theta_{s,i}$.

Figure 6 shows measured z_T/z_0 values from all available SHEBA summer sites plotted against the corresponding roughness Reynolds number from our bulk flux algorithm. As in Figs. 3 and 4, the plot shows both hourly values and bin averages. Except for the two lowest $R_{*,B}$ bins, which contain only 2 and 58 points, respectively, the bin averages agree very well with Andreas's (1987) model.

Figure 7 shows the comparable summer plot for z_Q/z_0. As in winter, we measured the latent heat flux only at one height on the ASFG tower. Except for the lowest two $R_{*,B}$ bins, which contain only 6 and 33 values, respectively, the bin averages in Fig. 7 agree quite well with Andreas's (1987) theoretical model for z_Q/z_0.

We consequently retain (4.2) as our algorithm for predicting z_T/z_0 and z_Q/z_0 over summer sea ice, too.

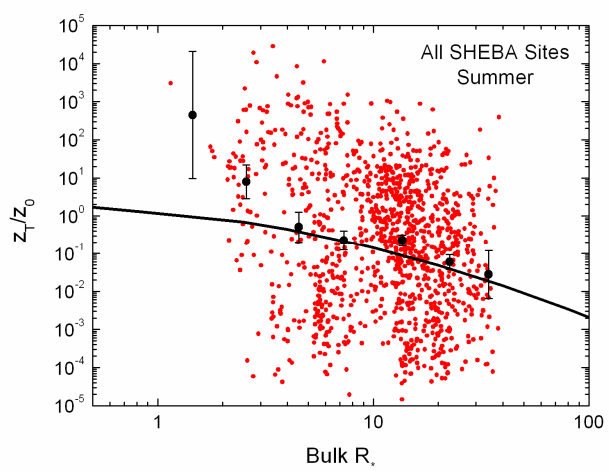

Fig. 6. Hourly z_T/z_0 measurements (red circles) from the SHEBA summer sites—ASFG tower, Atlanta, Baltimore, Florida, and Maui—are plotted against the roughness Reynolds number from our bulk flux algorithm, $R_{*,B}$. The figure summarizes 1177 such values. The black circles are geometric means within $R_{*,B}$ bins; the error bars are ±2 standard deviations in the bin means. The curve is (4.2).

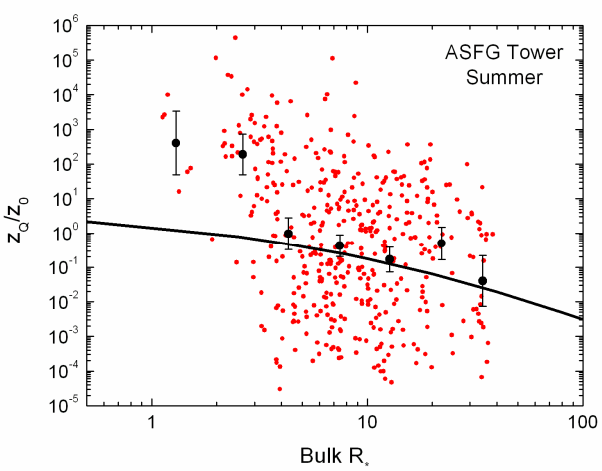

Fig. 7. As in Fig. 6, except this plot shows z_Q/z_0 from measurements only on the Atmospheric Surface Flux Group tower. This figure contains 439 hourly values.

6. SUMMARY

Our bulk flux algorithm for predicting the turbulent surface fluxes of momentum and sensible and latent heat over winter and summer sea ice consists of (2.1)–(2.7), (4.1), (4.2), and (5.3). It also requires the stratification corrections ψ_m and ψ_h, given in Paulson (1970) and Grachev et al. (2007) and some dynamic and thermodynamic variables, which we compute according to Andreas (2005).

Our algorithm's prediction for the drag coefficient over summer sea ice, (5.3), is also appropriate for any marginal ice zone. Because in winter marginal ice zones, at least, the surface temperatures of the ice and the open water will be much different, computing H_s and H_L here will probably require a mosaic-based calculation, like (5.6), where $\Theta_{s,Ave}$ is the areally weighted surface temperature. [And $Q_{s,Ave}$ would be the comparable areally weighted surface specific humidity for use in (2.1c).] We suspect, though, that C_{Hr} and C_{Er} can be calculated from (4.2) and (5.3), as we did over summer sea ice.

In closing, we have developed FORTRAN code for this algorithm and are willing to share it.

7. ACKNOWLEDGMENTS

The U.S. National Science Foundation (NSF) supported our initial participation in SHEBA with awards to the U.S. Army Cold Regions Research and Engineering Laboratory, NOAA's Environmental Technology Laboratory (now the Earth System Research Laboratory), the Naval Postgraduate School, and the Cooperative Institute for Research in Environmental Sciences. NSF also supported our use of the Flux-PAM stations from the facilities pool at the National Center for Atmospheric Research. Both NSF (award 06-11942) and the National Aeronautics and Space Administration (award NNX07AL77G) supported ELA at NorthWest Research Associates during the preparation of this manuscript.

8. REFERENCES

Anderson, R. J., 1987: Wind stress measurements over rough ice during the 1984 Marginal Ice Zone Experiment. *J. Geophys. Res.*, **92,** 6933–6941.

Andreas, E. L, 1987: A theory for the scalar roughness and the scalar transfer coefficients over snow and sea ice. B*ound.-Layer*

Meteor., **38,** 159–184.

____, 1998: The atmospheric boundary layer over polar marine surfaces. *Physics of Ice-Covered Seas,* Vol. 2, M. Leppäranta, Ed., Helsinki University Press, 715–773.

____, 2002: Parameterizing scalar transfer over snow and ice: A review. *J. Hydrometeor.*, **3,** 417–432.

____, 2005: *Handbook of Physical Constants and Functions for Use in Atmospheric Boundary Layer Studies. ERDC/CRREL Monogr.*, No. M-05-01, U. S. Army Cold Regions Research and Engineering Laboratory, 42 pp.

____, and A. P. Makshtas, 1985: Energy exchange over Antarctic sea ice in the spring. *J. Geophys. Res.*, **90**, 7199–7212.

____, W. B. Tucker III, and S. F. Ackley, 1984: Atmospheric boundary-layer modification, drag coefficient, and surface heat flux in the Antarctic marginal ice zone. *J. Geophys. Res.*, **89,** 649–661.

____, C. W. Fairall, P. S. Guest, and P. O. G. Persson, 1999: An overview of the SHEBA atmospheric surface flux program. Preprints, *Fifth Conf. on Polar Meteorology and Oceanography*, Dallas, TX, Amer. Meteor. Soc., 411–416.

____, P. S. Guest, P. O. G. Persson, C. W. Fairall, T. W. Horst, R. E. Moritz, and S. R. Semmer, 2002: Near-surface water vapor over sea ice is always near ice saturation. *J. Geophys. Res.*, **107,** 8032, doi: 10.1029/2000JC000411.

____, C. W. Fairall, A. A. Grachev, P. S. Guest, T. W. Horst, R. E. Jordan, and P. O. G. Persson, 2003: Turbulent transfer coefficients and roughness lengths over sea ice: The SHEBA results. Preprints, *7th Conf. on Polar Meteorology and Oceanography*, Hyannis, MA, Amer. Meteor. Soc., 3.11.

____, R. E. Jordan, P. S. Guest, P. O. G. Persson, A. A. Grachev, and C. W. Fairall, 2004: Roughness lengths over snow. Preprints, *18th Conf. on Hydrology*, Seattle, WA, Amer. Meteor. Soc., JP4.31.

____, P. O. G. Persson, R. E. Jordan, T. W. Horst, P. S. Guest, A. A. Grachev, and C. W. Fairall, 2005: Parameterizing the turbulent surface fluxes over summer sea ice. Preprints, *8th Conf. on Polar Meteorology and Oceanography*, San Diego, CA, Amer. Meteor. Soc., J1.15.

____, K. J. Claffey, R. E. Jordan, C. W. Fairall, P. S. Guest, P. O. G. Persson, and A. A. Grachev, 2006: Evaluations of the von Kármán constant in the atmospheric surface layer. *J. Fluid Mech.*, **559,** 117–149.

____, P. O. G. Persson, and J. E. Hare, 2008: A bulk turbulent air-sea flux algorithm for high-wind, spray conditions. *J. Phys. Oceanogr.*, **38,** 1581–1596.

____, ____, R. E. Jordan, T. W. Horst, P. S. Guest, A. A. Grachev, and C. W. Fairall, 2009: Parameterizing turbulent exchange over sea ice in winter. *J. Hydrometeor.*, submitted.

Birnbaum, G., and C. Lüpkes, 2002: A new parameterization of surface drag in the marginal ice zone. *Tellus,* **54A,** 107–123.

Briegleb, B. P., C. M. Bitz, E. C. Hunke, W. H. Lipscomb, M. M. Holland, J. L. Schramm, and R. E. Moritz, 2004: Scientific description of the sea ice component in the Community Climate System Model, version three. NCAR Tech. Note NCAR/TN-463+STR, 70 pp.

Brunke, M. A., M. Zhou, X. Zeng, and E. L Andreas, 2006: An intercomparison of bulk aerodynamic algorithms used over sea ice with data from the Surface Heat Budget for the Arctic Ocean (SHEBA) experiment. *J. Geophys. Res.*, **111,** C09001, doi: 10.1029/2005JC002907.

Claffey, K. J., E. L Andreas, D. K. Perovich, C. W. Fairall, P. S. Guest, and P. O. G. Persson, 1999: Surface temperature measurements at SHEBA. Preprints, *Fifth Conf. on Polar Meteorology and Oceanography*, Dallas, TX, Amer. Meteor. Soc., 327–332.

Deardorff, J. W., 1970: Convective velocity and temperature scales for the unstable planetary boundary layer and for Rayleigh convection. *J. Atmos. Sci.*, **27,** 1211–1213.

Fairall, C. W., E. F. Bradley, D. P. Rogers, J. B. Edson, and G. S. Young, 1996: Bulk parameterization of air-sea fluxes for Tropical Ocean-Global Atmosphere Coupled-Ocean Atmosphere Response Experiment. *J. Geophys. Res.*, **101,** 3747–3764.

____, ____, J. E. Hare, A. A. Grachev, and J. B. Edson, 2003: Bulk parameterization of air-sea fluxes: Updates and verification for the COARE algorithm. *J. Climate*, **16,** 571–591.

Garratt, J. R., 1992: *The Atmospheric Boundary Layer*. Cambridge University Press, 316 pp.

Godfrey, J. S., and A. C. M. Beljaars, 1991: On the turbulent fluxes of buoyancy, heat and moisture at the air-sea interface at low wind speeds. *J. Geophys. Res.*, **96,** 22,043–

22,048.

Grachev, A. A., C. W. Fairall, P. O. G. Persson, E. L Andreas, and P. S. Guest, 2005: Stable boundary-layer scaling regimes: The SHEBA data. *Bound.-Layer Meteor.*, **116,** 201–235.

____, E. L Andreas, C. W. Fairall, P. S. Guest, and P. O. G. Persson, 2007: SHEBA flux-profile relationships in the stable atmospheric boundary layer. *Bound.-Layer Meteor.*, **124,** 315–333.

Guest, P. S., and K. L. Davidson, 1987: The effect of observed ice conditions on the drag coefficient in the summer East Greenland Sea marginal ice zone. *J. Geophys. Res.*, **92,** 6943–6954.

Horst, T. W., S. P. Oncley, and S. R. Semmer, 1997: Measurement of water vapor fluxes using capacitance RH sensors and cospectral similarity. Preprints, *12th Symp. on Boundary Layers and Turbulence*, Vancouver, B.C., Amer. Meteor. Soc., 360–361.

Jordan, R. E., E. L Andreas, and A. P. Makshtas, 1999: Heat budget of snow-covered sea ice at North Pole 4. *J. Geophys. Res.*, **104,** 7785–7806.

Maykut, G. A., 1978: Energy exchange over young sea ice in the central Arctic. *J. Geophys. Res.*, **83,** 3646–3658.

Militzer, J. M., M. C. Michaelis, S. R. Semmer, K. S. Norris, T. W. Horst, S. P. Oncley, A. C. Delany, and F. V. Brock, 1995: Development of the prototype PAM III/Flux-PAM surface meteorological station. Preprints, *9th Symp. on Meteorological Observations and Instrumentation*, Charlotte, NC, Amer. Meteor. Soc., 490–494.

Paulson, C. A., 1970: The mathematical representation of wind speed and temperature profiles in the unstable atmospheric surface layer. *J. Appl. Meteor.*, **9,** 857–861.

Persson, P. O. G., C. W. Fairall, E. L Andreas, P. S. Guest, and D. K. Perovich, 2002: Measurements near the Atmospheric Surface Flux Group tower at SHEBA: Near-surface conditions and surface energy budget. *J. Geophys. Res.*, **107,** 8045, doi: 10.1029/2000JC000705.

Uttal, T., and 27 others, 2002: Surface Heat Budget of the Arctic Ocean. *Bull. Amer. Meteor. Soc.*, **83,** 255–275.

Vihma, T., 1995: Subgrid parameterization of surface heat and momentum fluxes over polar oceans. *J. Geophys. Res.*, **100,** 22,625–22,646.